

# High Altitude Atmospheric Turbulence

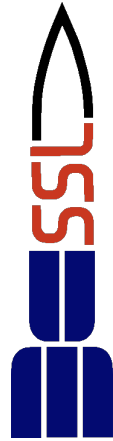
UMD HASP 2019 Flight Report

Flight 698N

December 13<sup>th</sup>, 2019



UNIVERSITY OF  
MARYLAND



University of Maryland, College Park  
Department of Aerospace Engineering  
Space Systems Laboratory (SSL)  
Hypersonic Aerodynamics and Propulsion Lab (HAPL)

Funding provided by the Maryland Space Grant Consortium

# Contents

<b>1</b>	<b>Project Overview</b>	<b>2</b>
1.1	Background and Scientific Objectives . . . . .	2
1.2	Previous HASP Missions . . . . .	3
<b>2</b>	<b>Payload Design</b>	<b>3</b>
2.1	Sensors and Data Acquisition . . . . .	4
2.2	Systems . . . . .	5
<b>3</b>	<b>Payload Location and Orientation</b>	<b>6</b>
3.1	Payload Position on CSBF . . . . .	6
3.2	Neighboring Payloads . . . . .	7
<b>4</b>	<b>Flight Performance Summary</b>	<b>8</b>
<b>5</b>	<b>Flight Data Analysis</b>	<b>9</b>
5.1	Ambient Temperature and Pressure Data . . . . .	9
5.2	Velocity and Temperature Fluctuation Data . . . . .	10
5.3	Pressure Fluctuation Data . . . . .	11
5.3.1	Identification of Acoustic Interference from Non-Atmospheric Sources . . . . .	11
5.3.2	Acoustic Interference from P10 . . . . .	16
5.3.3	Pressure Fluctuations from Atmospheric Sources . . . . .	17
<b>6</b>	<b>Recovery</b>	<b>17</b>
<b>7</b>	<b>Conclusions</b>	<b>18</b>
<b>A</b>	<b>Technical Drawings</b>	<b>20</b>
<b>B</b>	<b>Flight Time-line</b>	<b>22</b>
<b>C</b>	<b>HAAT Pre- and Post-Flight</b>	<b>23</b>
<b>D</b>	<b>Full Team Personnel for HASP 2019</b>	<b>24</b>
<b>E</b>	<b>Placement of Students from Past UMD HASP Teams</b>	<b>26</b>

# Abstract

The University of Maryland (UMD) 2019 HASP team combined the capability and fidelity of the High Altitude Atmospheric Turbulence (HAAT) payloads that previously flew in the 2017 and 2018 HASP flights. The objective of HAAT 2019 it to simultaneously obtain high frequency velocity, temperature, and acoustic fluctuation data. Such data represents a fundamental gap in knowledge which is necessary to aid in the prediction of boundary-layer transition for hypersonic vehicles. To this end, HAAT is equipped with hot-/cold-wire probes for unsteady velocity and temperature measurements, and high sensitivity microphones for measuring pressure fluctuations for frequencies above 10kHz. The wire probes enable the investigation of disturbance length-scales relevant to hypersonic boundary-layer instabilities; i.e. wavelengths on the order of millimeters to centimeters. HAAT operated as intended for the full duration of the flight, although more information in the telemetry during data acquisition would have been useful. Unfortunately both the hot- and cold-wire probes were damaged before data acquisition started, hence no temperature or velocity fluctuation data was collected; however, the microphone acquired several hours of pressure fluctuation data. Examination of this data emphasizes the sensitivity of our microphones to all ambient pressure fluctuations (and possibly mechanical vibration) as 99.4% of data is contaminated by non-atmospheric noise radiating from neighboring payloads. Such pressure fluctuations are on the order of  $0.05Pa$ , and largely dominate any atmospheric fluctuations; the noise floor of the microphones is  $0.004Pa$ .

The 2019 UMD HASP team included one graduate student, eight undergraduate students, and was project managed by a Post-Doctoral Associate working with Dr. Stuart Laurence. The team also includes two faculty advisers, Dr. Stuart Laurence and Dr. Mary Bowden. Dr. Mary Bowden has directed the Maryland Space Grant Balloon Payload Program for 16 years, launching over 90 soundings, three sounding rockets, and supporting seven previous HASP payloads.

# 1 Project Overview

## 1.1 Background and Scientific Objectives

Transition to turbulence of the boundary layers on the surface of a hypersonic flight vehicle brings with it a number of detrimental effects: a marked increase in surface heating levels (see Figure 1), elevated frictional drag, and large-amplitude pressure fluctuations that can couple with the structure of the vehicle and produce undesired oscillations. The prediction of transition in flight is thus of crucial importance in the vehicle design process. Transition is a highly complicated phenomenon and can follow several paths, depending on the intensity of the disturbance environment [1]. The conventional sequence for low-disturbance environments has freestream disturbances (vorticity, sound, and/or entropy spots) exciting normal modes within the boundary-layer through receptivity; these modes initially undergo linear growth until their amplitudes are sufficiently large that nonlinear effects take over, eventually resulting in breakdown and the formation of turbulent spots. These then merge to produce a fully turbulent boundary-layer. This process can be influenced by a number of operational modifiers, for example, surface roughness. While substantial progress has been made recently in understanding both various parts of this sequence and the overall transition process using theory, numerical simulations, and ground testing, extrapolation to flight requires knowledge of the flow disturbance environment likely to be encountered by hypersonic vehicles.

Unfortunately, while hypersonic ground testing is orders-of-magnitude less expensive than flight testing, experiments in traditional ground-test facilities are compromised by the presence of much higher freestream disturbance levels than in flight, which can strongly affect the location of the onset of turbulence [3, 4, 5]. This has led to the development of quiet (low-disturbance) tunnels [6], which are believed to have similar disturbance levels to those found in flight (though in the absence of detailed atmospheric measurements, this remains an assumption); however, the current generation of quiet tunnels is unable to achieve sufficiently high Reynolds numbers to produce natural transition on geometries of interest [4]. The extrapolation of transition locations from ground testing to flight thus must be performed through some kind of prediction methodology. Basic amplitude ratio (or  $e^N$ ) methods have found extensive use due to their simplicity, but, as pointed out by Reshotko [1], are ‘*defective in principle and perhaps also in practice,*’ as they do not accommodate the disturbance environment; the importance of which should be clear from the description in the previous paragraph.

In 1976, Reshotko’s [1] review article on boundary-layer stability and transition expressed pessimism regarding the prediction of transition in flight due to the lack of information of the disturbance environment at relevant altitudes. Hypersonic flight will typically take place in the range of 24-60km ( $\approx$  80-200kft), *i.e.*, in the upper stratosphere and lower mesosphere. Such altitudes are generally beyond the limits accessible by aircraft-based measurement; for example, the U2-based HICAT program [7] was restricted to 70kft, the SR-71 Blackbird was capable of altitudes up to 90kft [8, 9], and more recently the Perlan-Airbus high altitude glider reached 76kft in September 2018 [10, 11]. In the years since Reshotko [1], however, a number

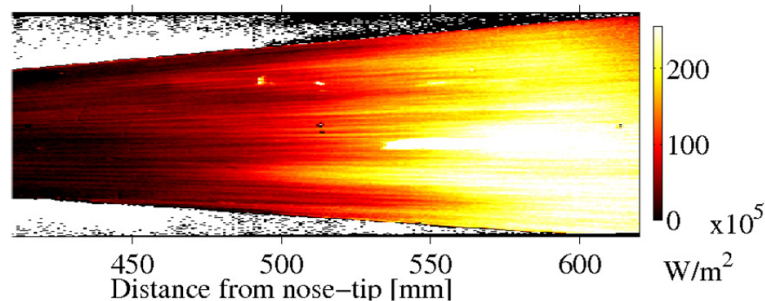


Figure 1: Heat-flux distribution measured on the surface of a slender cone at Mach 7.5 [2]. The marked increase in heat flux is caused by transition to turbulence of the boundary layer.

of balloon- and sounding-rocket-based measurements have probed the upper atmosphere: balloons are able to achieve altitudes typically in the range of 80-150kft [12, 13, 14, 15, 16], while sounding rockets are used for higher altitudes, e.g., [17]. Previous measurements have primarily been carried out by atmospheric physicists, with the intent of obtaining geophysical information regarding clear air turbulence (CAT) at these altitudes to improve our knowledge of atmospheric processes. Only recently have measurements focused on the small length scales (millimeters to centimeters) characteristic of hypersonic boundary layers and thus of relevance to the transition process. Nevertheless, a clear gap remains in knowledge/literature of the stratospheric turbulent environment to inform hypersonic boundary-layer transition predictions. Misinterpreted freestream disturbances can result in markedly enhanced thermal and mechanical loads compared to predictions (or alternatively, an over-designed thermal protection system) if not appropriately understood and taken into consideration for robust vehicle design.

Turbulence and associated natural processes play an important role within many aspects of the Earth's atmosphere, although, they are not fundamentally characterized or understood. Even within statically stable stratified environments, such as that observed in the stratosphere, turbulence occurs in layers of limited depth induced by the breaking of mountain waves (also referred to as gravity waves) and/or strong wind shears, which induce Kelvin-Helmholtz instabilities. Thus, the objective HASP 2019 is to provide an experimental demonstration of the ability to examine turbulent velocity, temperature, and acoustic fluctuation properties simultaneously, down millimeter length-scales in the stratosphere with a payload that can operate for extended periods of time. This will be achieved by utilizing a suite of hot-/cold-wires and high-sensitivity microphones.

## 1.2 Previous HASP Missions

UMD NearSpace's 2017 HAAT campaign successfully incorporated both hot-/cold-film instrumentation, and associated equipment into the first iteration of HAAT. This flight was primarily used to validate the measurement system for extended operations at high altitudes (up to 109kft); data was recorded at a sampling rate of 30kHz over a duration of 7 hours. Investigation of the turbulent velocity spectra indicated decays of  $-5/3$  (inertial sub-range) and  $-7$  (viscous sub-range) in regions of high disturbance, temperature spectra were not sensitive enough. Furthermore, during the HASP flight it was found that external structural components of the payload, made from 3D printed plastic, deformed. The payload did remain intact and data was not corrupted. The payloads suffered from thermal management issues causing the batteries to run cold and lose power faster than anticipated.

UMD NearSpace's 2018 HAAT campaign focused on acoustic measurements utilizing three different PCB microphones. Despite rigorous testing no data was recorded due to a failure to trigger the data acquisition system. The data acquisition system used in the HASP 2018 payload was the same as that used for the HASP 2017 payload. Inspection of the data acquisition system after the HASP 2018 flight indicated possible loose connections in the electronics.

## 2 Payload Design

A schematic for the HAAT payload is presented in figure 2. The main structural enclosure of the payload was fabricated from expanded polypropylene with a minimum wall thickness of 20mm. The base of the payload was secured to the HASP mounting plate using six M4 bolts, secured underneath the batteries through HAAT's reinforced mounting plates as indicated. The back plate could be completely removed to access HAAT's internal components, and housed 10mm thick cryogenic insulation inserts, the RS232 DB9 serial port, and the voltage regulator. The back plate itself was fabricated from 6.35mm thick polycarbonate sheet which supported and braced the EPP foam enclosure structure. A technical drawing of HAAT is provided in Appendix A.

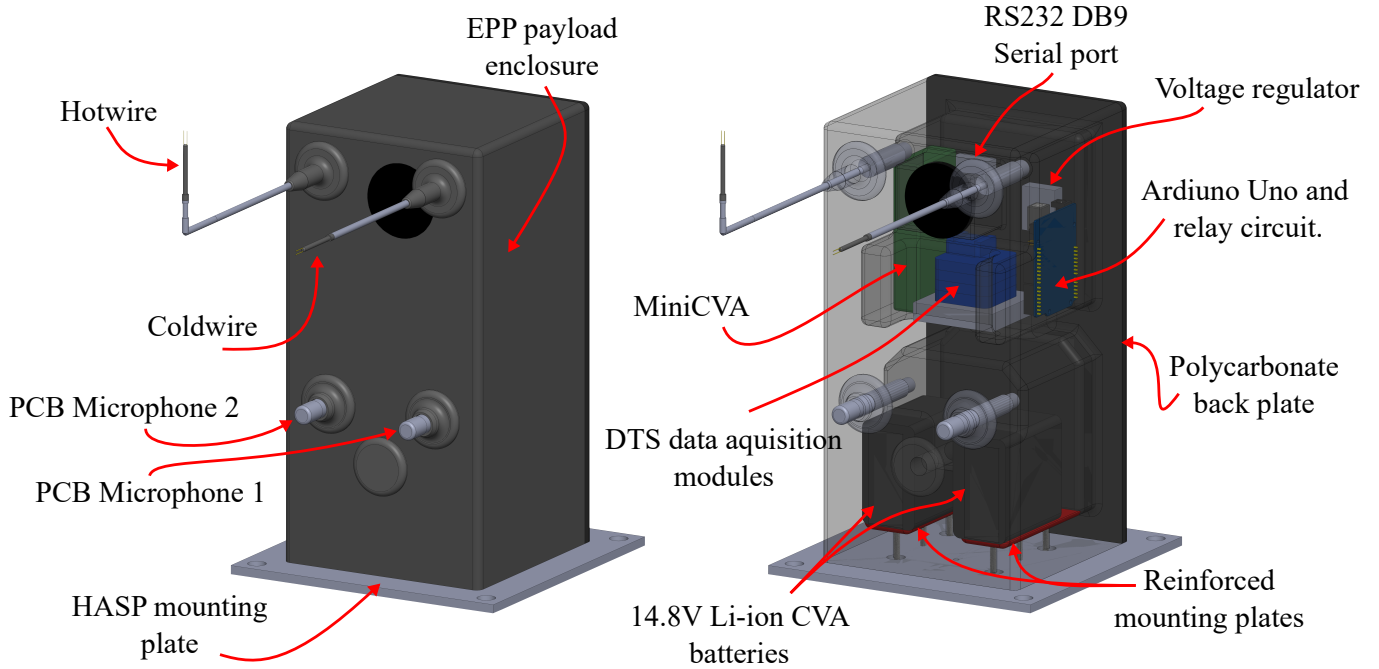


Figure 2: HAAT schematic diagram.

## 2.1 Sensors and Data Acquisition

Velocity fluctuations are observed using a single-wire constant voltage anemometer (CVA - also referred to as a hot-wire), where the measurement principle is based on the convective cooling caused by airflow over a heated fine wire. Temperature fluctuations are measured with a constant-voltage-biased temperature anemometer (CVT - also referred to as a cold-wire), where the wire resistance varies with the fluid temperature; essentially operating as a resistance temperature detector (RTD).

The two typical modes of operating wire anemometers are the constant current anemometer (CCA) and the constant temperature anemometer (CTA). In comparison to the CCA and CTA modes, the CVT and CVA offer advantages such as larger bandwidths, lower electrical noise, and higher sensitivity [18, 19]. Furthermore, Sarma [20] has theoretically shown, and Kegerise and Spina [21] have experimentally validated, that the bandwidth of the CVA does not change with overheat. This constant bandwidth feature of the CVA coupled with its demonstrated attributes of large bandwidth, low electronic noise, and high sensitivity make it extremely attractive for obtaining measurements from (near) sea-level conditions to high altitudes. The CVA/CVT anemometer channels are supplied by Tao Systems Inc. (Model 4-100 MiniCVA), offering a frequency response of  $50kHz$ . Each anemometer uses a TSI 1210 – T1.5 fine wire probe; the diameter and length of the platinum plated tungsten sensing wire are  $3.8\mu m$  and  $1.27mm$ , respectively. The probes are then held in place  $190mm$  in-front of HAAT using modified 1150 – 6 TSI probe supports. The hot-wire is un-calibrated in this work due to the bandwidth of conditions; however, the cold-wire has been calibrated using the University of Maryland’s Envirotronics environmental thermal chamber (Model ST16) capable of reaching temperatures at low as  $-80^{\circ}C \pm 3^{\circ}C$ ; the CVT mode, like the CCA, is not sensitive to changes in pressure or velocity.

HAAT is also equipped with two PCB Piezotronics microphones of the same type: a PCB 378A04 (sensitivity  $450mV/Pa$ ; frequency range,  $\pm 2dB$ , 10 to 16,000Hz). The 378A04 microphones points directly forward out of HAAT, away from the main CSBF gondola (see figure 4). It is noted that microphone 1 was configured for measurements of pressure fluctuations in the range of  $\pm 0.5Pa$ , while microphone 2 was configured for pressure fluctuations in the range of  $\pm 1Pa$ . Additionally, for monitoring the ambient atmosphere during the float, there is an externally mounted K-type thermocouple and pressure transducer

(Endevco model 8515C-15). The payload also has an internally mounted K-type thermocouple as part of the payload health monitoring system (primarily in place to monitor the temperature of the 12 Tenergy Li-ion 18650 rechargeable cells for the MiniCVA). The hot-/cold-wires and microphone positions is indicated in figure 2.

All instrument data is recorded via a DTS SLICE MICRO data-acquisition system (DAS). This system offers a complete standalone data-acquisition solution providing sensor excitation, signal processing, and 16GB flash memory. DTS BRIDGE SLICES are used for the hot-/cold-wire channels, thermocouples and the pressure transducers, while a DTS IEPE SLICE integrates with the piezoelectric microphones. The DTS system can offer sampling rates up to 500kHz per channel; in this work, all of HAAT’s sensors are simultaneously sampled at 40kHz offer a total data acquisition time of 6.16 hours.

## 2.2 Systems

The schematic for the circuitry for HAAT payload is presented in figure 3. HASP power will be used to power the DAS due to the maximum current requirements imposed on the system. The power is first fed through a 10V regulator to power the End-of-Chain (EOC) terminals, which is used to power and trigger the DAS. Two 14.8V Li-ion batteries were used to power the MiniCVA and excite the fine-wire probe sensors; each of these batteries were Tenergy Li-ion 18650 14.8V 5200mAh rechargeable batteries.

The discrete pins  $F$  and  $N$  were intended to be used to trigger the MiniCVA once float altitude is reached, however, later designs demonstrated that controlling the three relay switches through serial commands was simpler and more robust to implement. The relays isolated the batteries from the MiniCVA until triggered at float altitude. This avoided expending finite battery life during ascent.

The Arduino UNO (utilizing HASP power) was used as HAAT’s main processing unit to facilitate interfacing with the HASP gondola, and communicate the status signal from the DAS. It’s main purpose was to parse and act upon different serial commands, as well as transfer telemetry back to the ground at 1Hz. The telemetry data indicated the state of the payloads functionality and what it was trying to do following commands from operators. The Arduino unit was capable to handling four serial commands including: arm; dis-arm; trigger, and ping. A list of these commands have been summarized in table 1. Once armed, and subsequently triggered, the relay switches connected the 10V output of the voltage regulator to the end-of-chain terminal, triggering the DAS systems. Simultaneously, two further relays

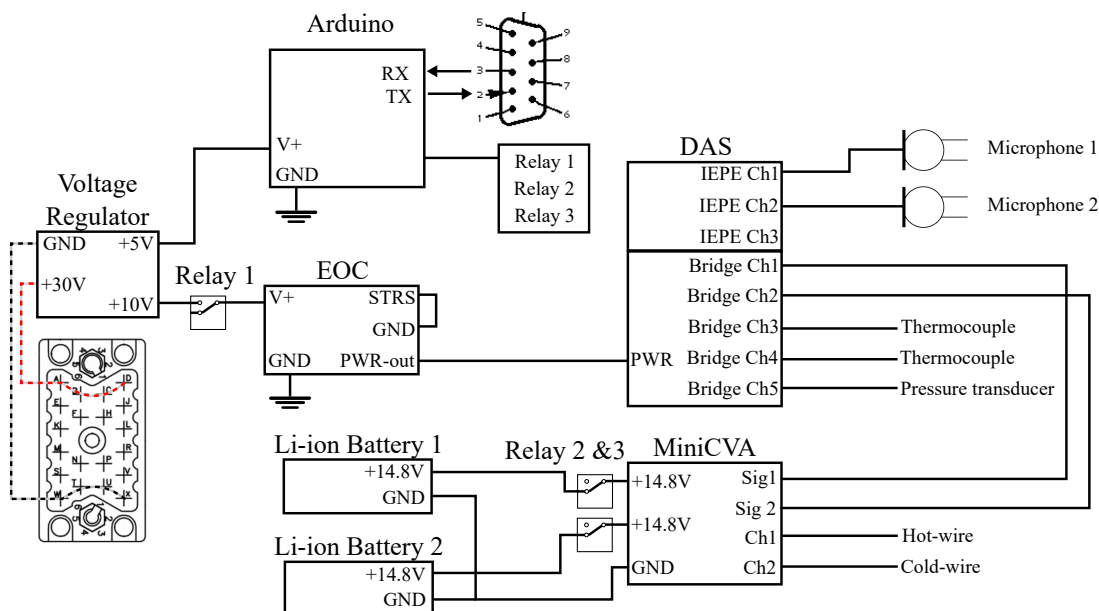


Figure 3: Schematic diagram of HAAT systems.

Command	Description	Character	Hex Code
Arm	Arms HAAT to prepare for data acquisition	A	0x00, 0x41
Dis-arm	Sets HAAT to an idle mode	D	0x00, 0x44
Trigger	Start data acquisition	T	0x00, 0x54
Ping	Ping HAAT to manually check status	P	0x00, 0x50

Table 1: Uplink command list.

were triggered to connect the 14.8V outputs of the Li-ion batteries to the MiniCVA. This design addresses design flaws in the electronics from HASP 2018. A full technical schematic of the electronics layout is provided in Appendix A.

### 3 Payload Location and Orientation

#### 3.1 Payload Position on CSBF

The majority of the experimental goals are independent of the physical location on the HASP gondola. The stern side of the gondola was deemed to be best suited logistically as it is situated farthest from the launch vehicle prior to launch [22]. However, two discrete lines were initially thought to be required by HAAT for activating and triggering the payload which is not accommodated by either payload locations 06 or 07 on the stern of the gondola. Hence payload location 05, as indicated in figure 4, was best suited HAAT’s requirements as suggested by the HASP reviewing committee.

The HAAT payload was orientated with probes pointing away from the main gondola (orientation shown in figure 4), and therefore had very fragile (and sharp) fine-wire probes pointing out beyond the ground footprint of the gondola. It was thought that having HAAT mounted at payload location 05, away from the launch vehicle, would minimize the chances of damaging the probes prior to launch. The approximate CSBF camera position on the gondola is also indicated in figure 4; there was no payload in position 12. It is noted that payloads 01, 02, 09, and 10, will be referred to at P01, P02, P09, and P10 respectively throughout the rest of this report.

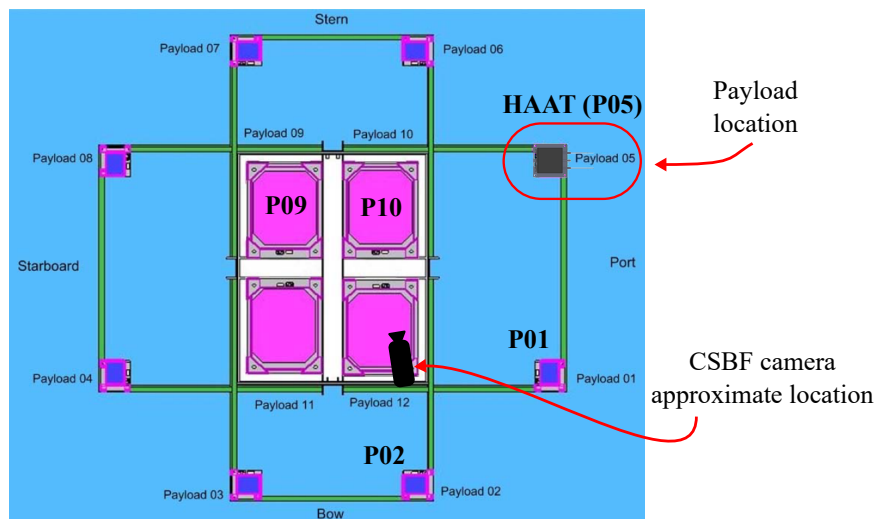


Figure 4: Payload location on the stern of the HASP gondola in position 05; payload orientation had probes pointing away from main gondola as shown. View is top down.

## 3.2 Neighboring Payloads

The results from HAAT have emphasized to our HASP team the need to understand the function and operations of neighboring payloads. Several payloads on the CSBF 698N flight operated with stepper motors, fans, and/or pumps. Figure 5 presents two frames from the CSBF live camera feed; unfortunately HAAT is not in the frame (HAAT is to the right of the field-of-view as indicated). P09 and P10 are located directly behind HAAT (see figure 4). Each of these payload's functional operations require stepper motors (one for P09, and two for P10), with figure 5 indicating the payloads motions with the blue arrows.

P09 activated its motor just before float was reached (at  $\approx 15:33:44$ ) to open and rotate the hatch on the top of the payload and deploy their experiment; this operation visible in figure 5. P09's stepper motor remained on for the full duration of the float, however it is understood that there were operational issues with the stepper motor and the experiment could now be re-stowed back inside the payloads before flight termination.

P10's pitch and yaw stepped motors were powered for the full duration of the flight (from launch), however, were not always attempting maneuvers and were also power cycled a couple of times during the flight. P10's motors are also noted to independently suffer from violent motor jitter periodically through the flight; this is apparent through observations made through CSBF's recorded live feed. The typical of motion for P10 is indicated by the blue arrows in figure 5. It is noted that when P10 is unable to lock onto and track the sun it performs a parallel track search pattern (also referred to as a lawnmower search pattern). Hence, when searching it yaws and pitches in an alternating pattern (start yaw, stop yaw, start pitch up, stop pitch up, start yaw, stop yaw, start pitch down, stop pitch down, etc.) with each motion lasting  $\approx 3$  seconds (assessed from CSBF camera feed).

The last payload which could potentially provide a significant source of acoustic noise is P01. P01 housed an assortment of fans and pumps necessary for their experimental analysis of particulates in the stratosphere. It is not known exactly how many small fans and pumps P01 housed or what their operating frequencies are. However, P01 has been confirmed to utilize a single 38mm 7-blade axial fan which is expected to operate between 6000 and 7000 RPM. This fan is used to provide payload cooling. The cooling fan and particulate counter fans were mounted vertically facing away from the main gondola (*i.e.* in the same direction as HAAT's sensor array). While the frequency signatures of P01 are not fully understood, it is known (through private communications) that the payload activated all of its particulate counter fans and pumps from  $\approx 12:33:00$  till  $\approx 16:21:38$ , and again from  $\approx 17:46:49$  till  $\approx 18:25:13$ . P01's 38mm axial cooling fan was active from  $\approx 15:35:41$  till  $\approx 16:21:38$ , and again from  $\approx 17:46:49$  till  $\approx 18:25:13$ . It is lastly noted that P01 shared the same outrigger on CSBF as HAAT, on the port side of the gondola as shown in figure 4.

A summary of potential sources of noise from neighboring payloads is presented in table 2. This

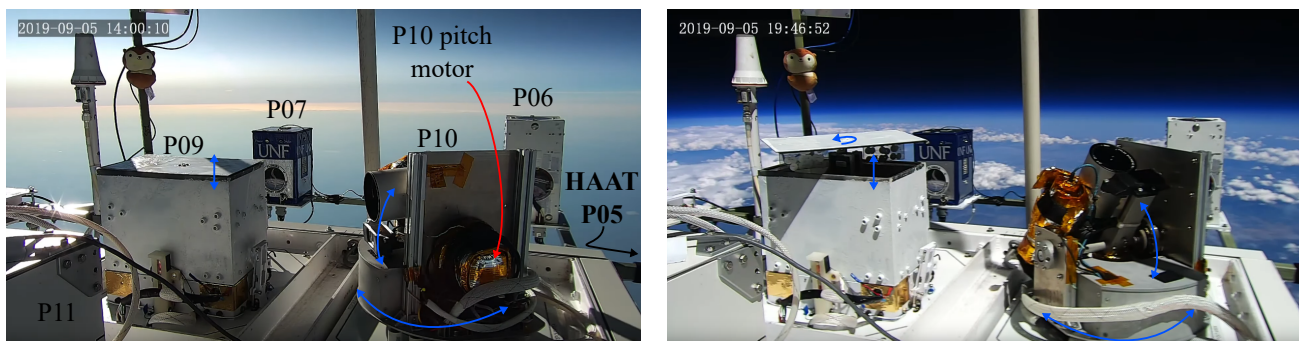


Figure 5: View from CSBF camera indicating several payload locations relative to HAAT; note that real time is shown in the top left of each frame. The blue lines indicate the motions (controlled by stepper motors) for payloads P09 and P10, which were positioned directly behind HAAT (P05) as shown in figure 4.

Payload	Potential Noise Source	Acoustic frequency	Anticipated Interference
P01	Multiple fans and pumps	unknown	Med/High
P01	38mm, 7-blade axial fan	$\approx 117Hz$	Med/High
P02	Pump ( $\times 1$ )	unknown	Low
P09	NEMA 14 stepper motor ( $\times 1$ )	$\approx 71.4Hz$	Low
P10	NEMA 17 stepper motor ( $\times 2$ )	300Hz to 1000Hz	High
P10	Yaw and pitch drive trains ( $\times 2$ )	unknown	High
P10	Pitch motor mounting structure	unknown	High

Table 2: Known potential sources of noise from neighboring payloads.

information has been collected through private communications with the respective HASP teams. It is noted that there will be additional sources of noise we are unaware of including structural natural frequencies of other payloads and the outrigger. There are also events such as the dropping of ballast which could acoustically generate noise.

## 4 Flight Performance Summary

HAAT operated as intended, successfully acquiring 5.19 hours of data at  $40kHz$  during the CSBF float - however there are modifications which would improve functionality of HAAT in future designs. The pre-allocation of HAAT's 16GB of flash memory embedded within the data acquisition system enabled a total record time of 6.16 hours in 10 minute segments (data was saved in this manner to navigate issues with HAAT in HASP 2018). Hence, 20 minutes of acquisition time was used during pre-flight bench and hang testing, thus leaving a total potential acquisition time of 5.83 hours for the flight. HAAT acquired data between 15:48:29 and 21:50:14 (6.03 hours), during which operators power cycled HAAT four times due to observed oscillations in the current draw. This led to a down-time of 50.4 minutes (0.84 hours). The power cycling accumulatively lost 23.94 minutes of potential data acquisition to memory pre-allocation. At 21:50:14, HAAT ran out of memory capacity and settling into an idle mode in which the data acquisition system and sensors were active but were not recording. The flight performance of HAAT is summarized in figure 6 which illustrates HAAT's voltage and current draw from launch (13:03:15) through the CSBF ascent and float, till the flight is finally terminated at 23:17:56.

For a total mission time of 7 hours and 37 minutes (7.62 hours), HAAT acquired data for 68% of the float (or for 89% of HAAT's maximum possible endurance), and functioned as intended for the whole flight

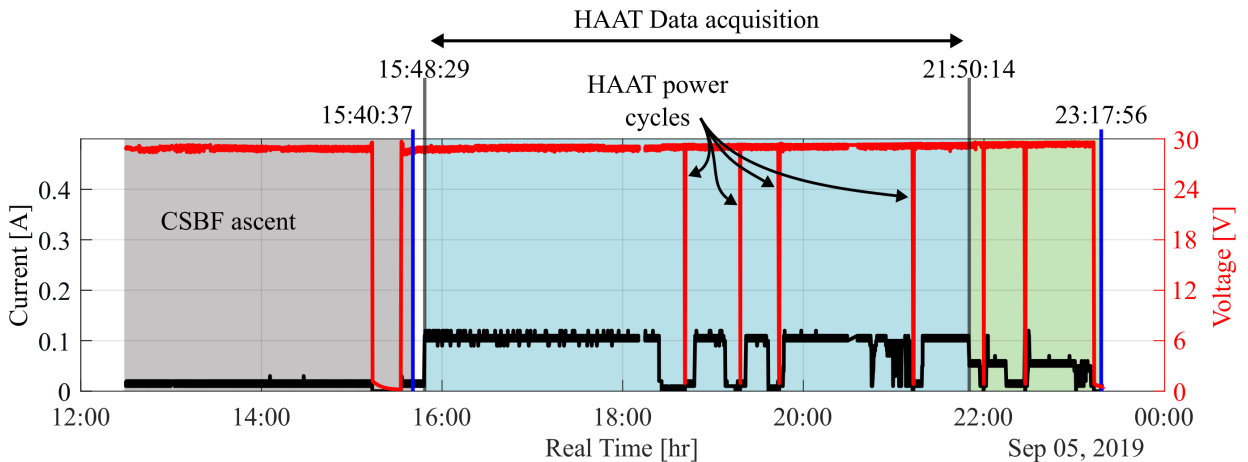


Figure 6: HAAT Voltage and Current Draw.

(bearing in mind that HAAT was idle towards the end of the flight for 1 hour 28 minutes, or 20% of the flight due to memory capacity limitations).

HAAT’s current draw was observed to drop to levels indicating the payload had shut-down all sensors and DAS at 18:24:10, 19:07:22, and 19:36:46, with oscillations in the current starting at 20:44:16. These current draw fluctuations prompted operators to follow payload power cycling procedures as outlines in the UMD team’s Flight Operations Plan (FLOP) at 18:41:06, 19:17:58, 19:43:43, and 21:12:38 (composing a total down-time of 50.4 min). However, in view of the data obtained by HAAT, it is not clear that the power cycling was necessary as the apparent drops in current draw do not correlate to any changes in data acquisition or sensor performance. In other words, the drop in current observed during the flight does not appear to be representative of the functional state of HAAT.

The data telemetry downlink for HAAT indicated that the payload was still operating as per the most recent serial command. This emphasizes a flaw with HAAT’s operation in that it’s limited telemetry downlink did not provide enough information to truly asses the state of the payload. In hind-sight, HAAT could (should) have had better downlinked telemetry to better inform the UMD team on the state of HAAT’s functionality. The current draw was intended to be the primary method for assessing the state of the payload, with the only information passed in telemetry communicating the state of the data acquisition system (either ‘OFF’, ‘ON’, or ‘ARMED’). When the current was observed to drop the telemetry continued to indicate that the DAS was active and recording, which could have been trusted, but the current draw observation was deemed to be a stronger indicator of the operational state of the payload at the time. A full breakdown of the flight time-line is provided in Appendix B.

Future HAAT payloads (or any payloads) should have better telemetry consisting of multiple avenues to assess the payloads level of functionality. HAAT’s scientific data itself cannot be downlinked through telemetry due to the high data rates ( $40kHz$  to  $50kHz$ ) and the nature of the DAS hardware, but other data and information can be passed through the telemetry to indicate the state of the payload and the level of operational performance.

## 5 Flight Data Analysis

### 5.1 Ambient Temperature and Pressure Data

During the period of float, HAAT acquired data from 15:48:29 till 20:50:14. The internal and external temperature of HAAT is displayed in figure 7 along side temperature data acquired by the CSBF gondola for the front, back, left and right solar shields.

At 15:48:29 the internal temperature of the payload is just above freezing at  $+0.42^{\circ}C$ , during the payload operation the internal temperature is observed to rise continuously until the end of HAAT’s operations at 21:50:14 with a final internal temperature of  $+46.77^{\circ}C$ . Between 15:48:29 and 17:30:00, the

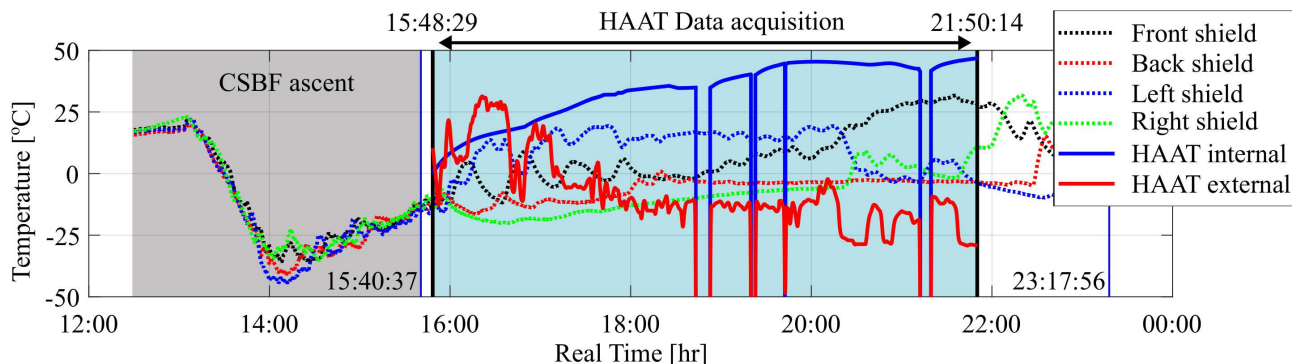


Figure 7: Mean temperature data measured by HAAT and CSBF.

internal temperature rises at a rate of  $\approx 0.5^{\circ}\text{C}/\text{min}$ . After which, the rate of heating plateaus towards  $\approx 0.08^{\circ}\text{C}/\text{min}$ ; this is possibly due to the power cycles reducing the rate of heating. The observations of the internal temperature variation with time suggests that the thermal management of HAAT is too aggressive. The combined internal passive heating (mostly from the CVA) in addition to the and the 20mm thick EPP structural walls lined layered cryogenic insulation is perhaps excessive.

The external temperature measurements indicate that the sensing element of the K-type thermocouple is too close to the surface of the payload and thus is not registering to true ambient temperature (the sensing element was  $\approx 40\text{mm}$  away from the surface). Considering the first portion of variations in the external temperature, between 15:48:29 and 17:16:15, there are distinct temperature oscillations detected by the external thermocouple (reaching up to  $+31^{\circ}\text{C}$  at 16:20:54). By assessing the CSBF live feed positive gradients in the temperature start as the port-side of the gondola turns to face the Sun, where peak temperatures are experienced as the port-side is directly facing the Sun (*i.e.* HAAT is facing the Sun). The temperature then immediately begins to fall again as the gondola continues rotating, and the port-side of the gondola turns away from the Sun. The approximate circumferential position of the Sun is determined through examinations of shadows cast by other payloads and other gondola protuberances.

The ambient pressure monitored by HAAT and CSBF is presented in figure 8. The mean atmospheric pressure measured by HAAT between 15:48:29 and 21:50:14 is 9.79mbar.

## 5.2 Velocity and Temperature Fluctuation Data

The hot- and cold-wires were both broken when HAAT began data acquisition at 15:48:29, hence no velocity or temperature fluctuation data was obtained. It is noted that monitored power consumption from the inboard batteries, and the voltages observed by the DAS indicate that the HAAT operated as intended and that the sensors were appropriately triggered and excited. The wire probes could have been damaged at any point between the hanger, on the 4<sup>th</sup> September when the wires were installed, and launch on the morning of the 5<sup>th</sup> September. It is also possible that launch itself damaged the wires. In 2017 HAAT flew disposable hot- and cold-film probes (TSI model 1201-20). These were substantially most robust at the expense of sensitivity; the sensing wire element had a diameter of  $50.8\mu\text{m}$  for the film probes, apposed to the  $3.8\mu\text{m}$  diameter for the fine-wire probes. It is noted that the fine-wire probes successfully flew on six sounding flights in 2019, with the payload landing in trees and lakes without the wires breaking.

Photographs of HAAT pre- and post-flight are shown in Appendix C indicating the position of the wires probes. On recovery it is indicated that a white ribbon (maybe duct-tape) is tangled around the probe supports, this too may have damaged the wire probes.

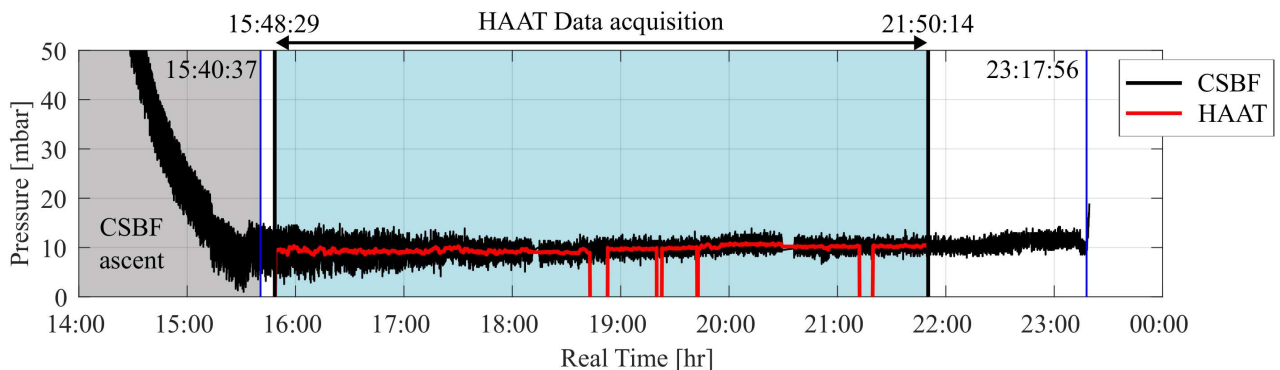


Figure 8: Mean pressure data measured by HAAT and CSBF.

## 5.3 Pressure Fluctuation Data

### 5.3.1 Identification of Acoustic Interference from Non-Atmospheric Sources

Acoustic interference from nearby sources, while troublesome in nature, have also served to demonstrate the high sensitivity of HAAT’s acoustic measurements at high altitudes. Of the full 5.19 hours of acquired data, there is 115 seconds of data which is not contaminated by non-atmospheric noise. An additional 50 seconds of data is partially contaminated. Unfortunately, over these 165 seconds (spaced over three events of duration 50, 10, and 105 seconds) there are no distinct atmospheric pressure fluctuations; the noise floor of the 378A04 microphones are  $\pm 0.004 Pa$  ( $\pm 4 \times 10^{-5} mbar$ ). It is noted that all data has been anti-alias filtered at  $20 kHz$  (Nyquist Theorem), and high-pass filtered at  $3 Hz$  to remove any low frequency acoustics induced by motions of the gondola.

The periods of time identified as ‘quiet’ were tracked by monitoring the root-mean-square of the pressure fluctuations and the maximum pressure fluctuations over 1 second increments. Comparison of the measured acoustics to the CSBF recorded live feed and the voltages/currents draw of neighboring payloads leads to compelling evidence that P01 and P10 are the primary sources of acoustic noise, with P09 possibly emitting noise too. Through private communications with the respective HASP teams we are able to anticipate what frequencies of noise can be expected (see Section 3). However, we can only speculate what additional frequencies may occur due to payload structural vibrations generating noise. For example, in the live feed P10’s structure can be seen to vibrate quite violently at times due to jitter in the pitch stepper motor.

The first period of quiet observed by HAAT occurs shortly after float is reached at 15:52:28; the pressure fluctuation data from microphone 2 is shown in figure 9. From figure 9 a distinct gap in the acoustic noise is observed for 50 seconds. Referring to the current draw data obtained by CSBF over the same time period, it is noted that P10’s current draw falls off at 15:52:28, coming partially back up at 15:52:50 (indicative of a power cycle which is confirmed through inspection of P10’s supply voltage), and returning to nominal draw at 15:53:18. This is illustrated in figure 10. Personal communication with P10’s team confirm that the

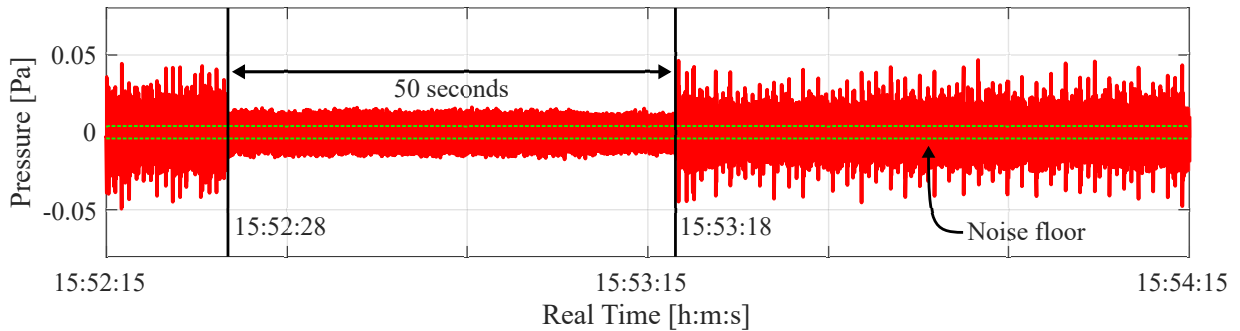


Figure 9: Pressure fluctuation data from microphone 2 between 15:52:15 and 15:54:15. The green dashed lines indicate the sensor noise floor at  $\pm 0.004 Pa$ .

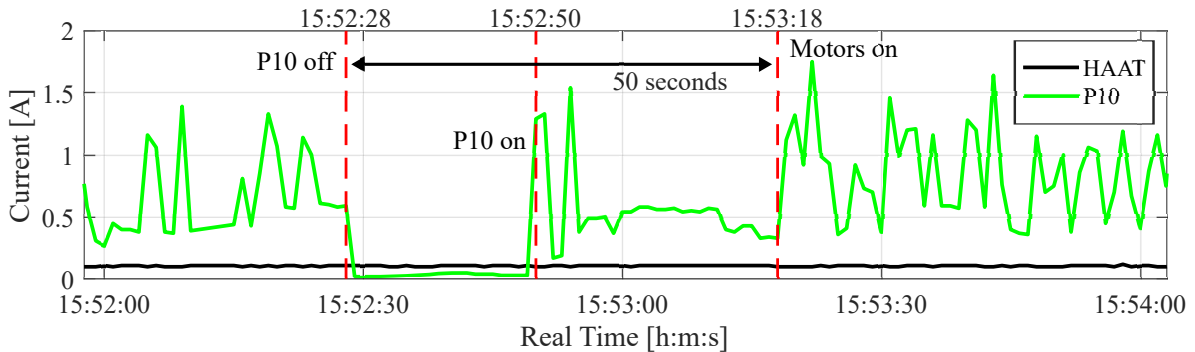


Figure 10: Current draw for HAAT and P10 over the 50 second quiet event shown in figure 9.

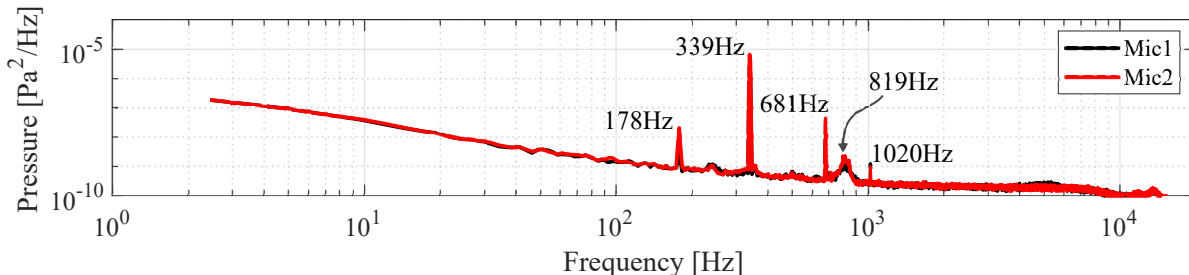
payload was cycled at this time. Furthermore, inspection of the CSBF recorded feed shows P10 pitching back and forth due to motor jitter before the power cycle at 15:52:14, at which point the jitter stops. Exactly 50 seconds later at 15:53:04, P10 begins to move in yaw again. Note that there seems to be an  $\approx 14s$  lag between the CSBF recorded video feed and the CSBF/HAAT data acquisition.

The spectra for both microphones 1 and 2 over 20 seconds at 15:52:30, and a minute later at 15:53:30 are presented in figures 11a and 11b, respectively. Acoustic noise linked to P10 activity lies in the range of  $200Hz$  to  $1000Hz$ . It has been established that between 15:52:28 and 15:53:18 P10 was not making any acoustic noise, thus it is curious that very specific frequencies are observed over the 50 seconds that P10 is inactive. These frequencies are visible within the spectra shown in figure 11a. Here, there are four main frequencies observed at  $178Hz$ ,  $339Hz$ ,  $681Hz$  and  $819Hz$ ; the fifth frequency observed is a harmonic due to acoustic interactions ( $339Hz + 681Hz = 1020Hz$ ).

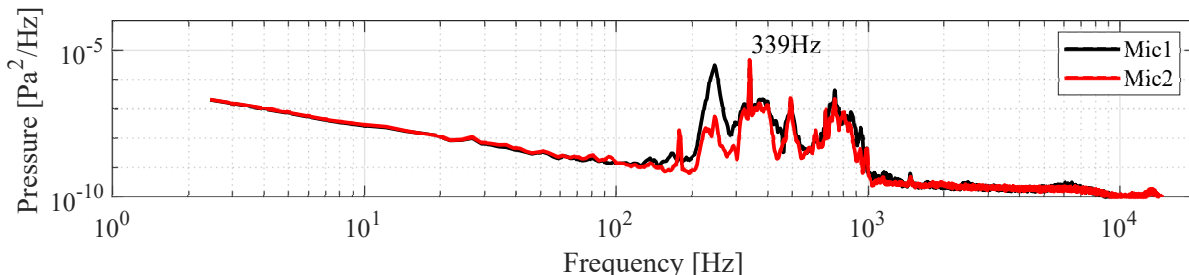
From these interactions the  $819Hz$  frequency is of immediate interest as it can be correlated to activity of P01's cooling fan (active between 15:35:41 till 16:21:38), and is known to operate at  $\approx 117Hz$ . Hence, with a 7-bladed fan, the passing frequency can be expected to be  $\approx 819Hz$ . The other frequencies observed do not have as well prescribed sources, however, they too can be attributed to the activity of P01. It is known through private communication, and the current draw of P01, that the payload stopped all experimental operations at about 16:21:38. Hence, if we compare spectra for pressure fluctuation data either side of this time, say 16:20:00 and 16:22:00, we can observe that these frequencies are linked to P01's operations; this is shown in figure 12 where spectral peaks are observed to disappear once P01 ceases activity. These spectral peaks are observed to intermittently return between 17:46:49 and 18:25:13, coinciding with P01 operations. The intermittency may suggest that P01 was having functionality issues, causing the fan to start/stop, but this cannot be confirmed based on the acoustic data.

For figure 12, it is noted that spectra are calculated over 20 seconds using Welch's method, and that P10 is active and accountable for the majority of the acoustic noise in both cases. Lastly, it is important to acknowledge that P01 was installed on the same outrigger as HAAT, as shown in figure 4. Thus, it is plausible that vibrations from P01 were transferred mechanically through the outrigger structure to HAAT, and subsequently detected by the microphones mechanically. This could also be true for vibrations from P10.

A second event of quiet detected by HAAT for 105 seconds occurred again much later in the flight at



(a) Quiet, 15:52:30 over 20 seconds.



(b) P10 back on, 15:53:30 over 20 seconds.

Figure 11: Pressure fluctuations spectra for P10 off at 15:52:30.

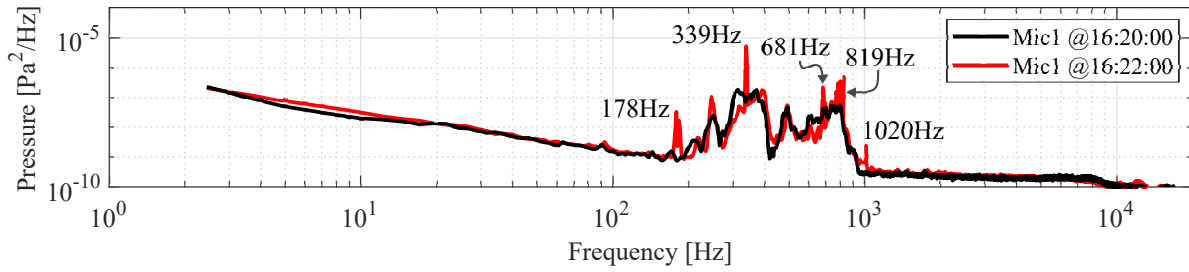
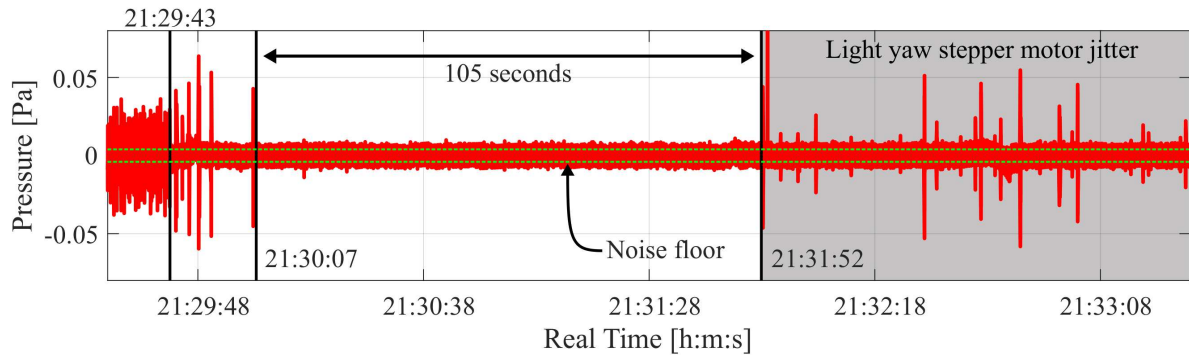


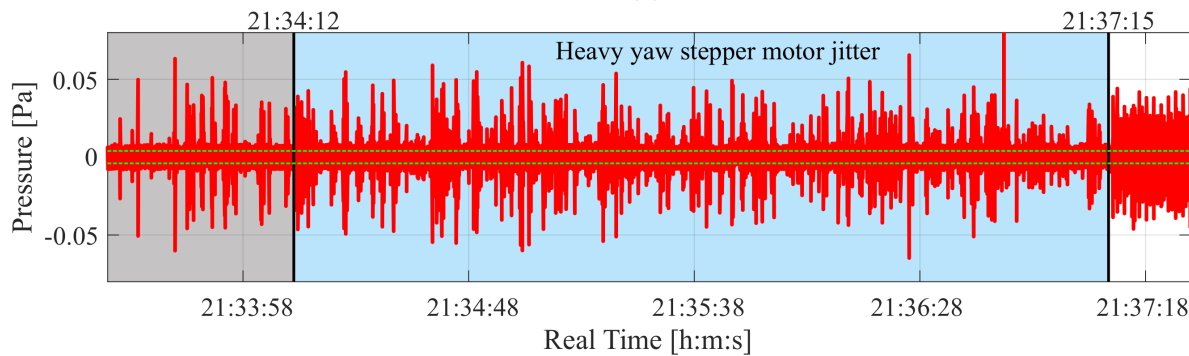
Figure 12: Pressure fluctuation spectra from 16:20:00 with both P01 and P10 payloads actively generating acoustic noise, and from 16:22:00 with P01 turned off and P10 continuing activity.

21:30:07. This period of quiet was preceded by several seconds of pulsed pressure fluctuations with no discernible pattern, and followed by several minutes of similar acoustic pulses which gradually grow in frequency (but with no particular pattern) until the nominal background noise returned. It is also noted that the peak amplitude of the fluctuations remains fairly constant. This entire event started at 21:29:43, and lasted 7 minutes 32 seconds, ending at 21:37:15. The pressure fluctuation data observed by microphone 2 over this time is presented in figure 13. It is indicated that payload P01 was not active over this time period.

With reference to figure 13, consider the current draw from P10 over the same time period shown in figure 14. P10 was not power cycled, but the current is observed to drop down to  $\approx 0.27A$  for 105s starting at 21:30:07 - a direct coloration to what was seen in the microphone data. Between 21:29:43 and 21:30:07, and again from 21:31:52 till 21:34:12, the current draw from P10 sits around  $\approx 0.27A$  but with several arbitrary spikes in the current draw occurring. From 21:34:12, these current spikes increase in frequency which parallel the increased, and sporadic, noise recorded by HAAT's microphones.



(a)



(b)

Figure 13: Pressure fluctuation data from microphone 2 between 21:29:43 and 21:37:18. The green dashed lines indicate the sensor noise floor at  $\pm 0.004Pa$ .

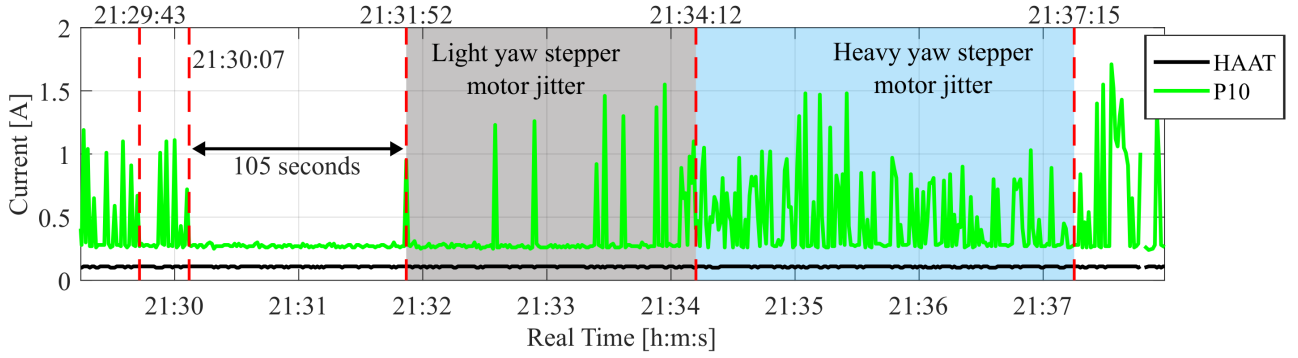


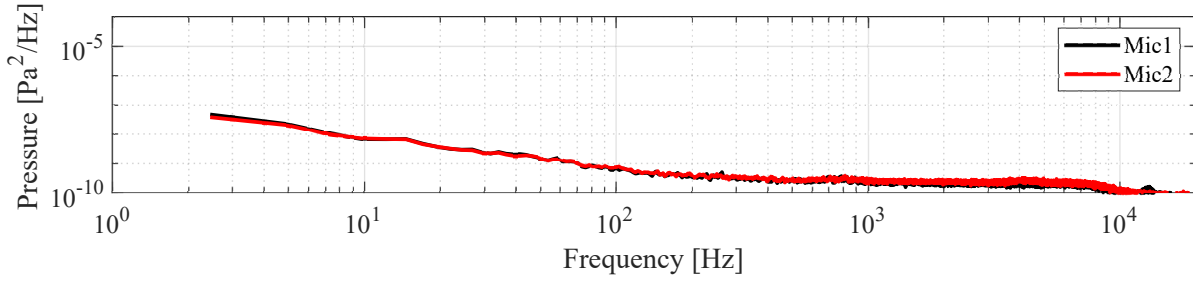
Figure 14: HAAT and P10 current draw between 21:29:43 and 21:37:15.

Through private communications with P10’s team, it was confirmed that issues were arising with the yaw motor and, due to this, several commands to attempted to rectify yaw motor issues were sent over this period of time. These commands attempted to set specific yaw potions to stop the sporadic motions of the motor and try facilitate a re-calibration of the yaw position. From the CSBF recorded live feed, P10 is observed to move in yaw for the first time in several minutes at 21:29:48. P10 is then observed to suffer from yaw motor jitter which stop around 21:30:05. Following this, at 21:31:10, P10 starts to jitter in yaw again moving slowly in a counter clockwise direction (looking down). At 21:33:51, the jitter motions increase in both frequency and duration, now twitching back and forth, leading to a quantitative assessment of maximum jitter activity at  $\approx 21:35:10$ . The payload continues to twitch back and forth until 21:37:19, at which point all motion stops. At 21:37:19 P10 smoothly yaws through  $\approx 45^\circ$  counter clockwise (looking down), and stops moving. These observations of jitter in the yaw motor last 7 minutes  $\approx 31$  seconds and can be coordinated with acoustic activity detected by the microphones. No further motion is observed again until 21:57:19 (HAAT stopped recording at 21:50:14).

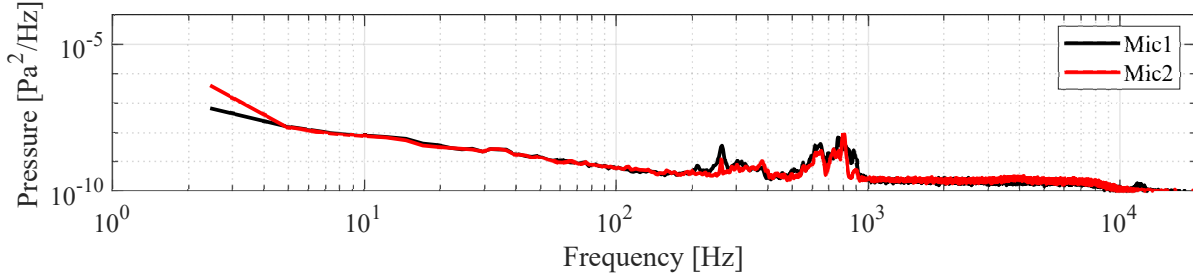
From figure 13 we can assess different spectra content produced by P10 (including the absence P10’s activity). This is shown in figure 15 which presents spectra from times periods were P10 was off (figure 15a), suffering from heavy yaw motor jitter (figure 15b), and back to nominal conditions for the flight (figure 15c). With P10 inactive we observe that any atmospheric pressure fluctuations are near the noise floor of the microphones, with no distinct pressure fluctuations observed over the uncontaminated 105 seconds. The period of time with motor jitter demonstrates similar acoustic frequencies from P10 under nominal operating conditions, but with a reduced amplitude. With P10 returning to normal operating conditions for this flight from 21:37:15 (figure 15c), a spectral peak at  $71Hz$  is noticed.

The  $71Hz$  is particularly difficult to identify a source for due to its inherent intermittent over the full duration of HAAT’s data acquisition. It appears for several minutes at a time during the flight and is always well defined; figure 16 illustrates the  $71Hz$  peak with the typical P10 spectral activity, and with P01 inactive. It would initially seem that the  $71Hz$  frequency is in someway connected to the activity of P10; however, it was previously noted in Section 3 that P09 operated a single stepper motor at  $\approx 71.4Hz$ . This motor was intended to operate continuously from 15:33:44 till 23:17:56, and was known to be unable to perform all of its intended operations during the flight, through private communication. The CSBF life feed also shows P09 failing to retract its experiment before flight termination. While there is not enough evident to correlate the  $71Hz$  frequency to P09, there is sufficient evident to suggest that P09 is indeed the source.

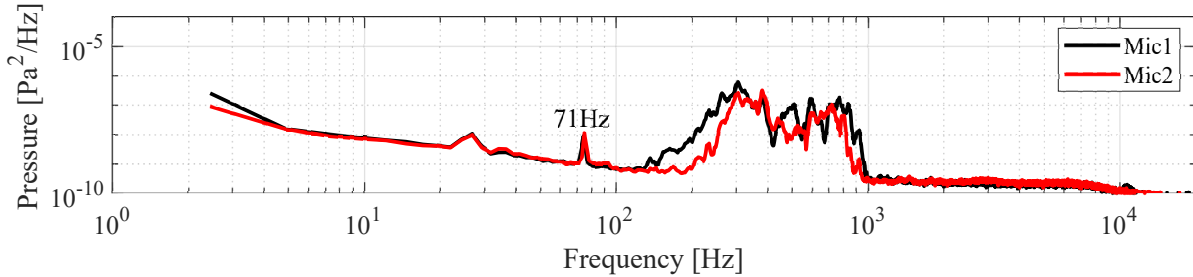
In consideration of the stepper motors on P09 and P10, it is necessary to emphasize that the motors do not need to be moving to generate acoustics. This is largely the case observed with P10, in which there is no obvious acoustic difference between the stepper motors holding position and moving. With particular attention to P10, as it’s motions are more directly observable through the CSBF feed and can be compared to the payload’s current draw, it seems that the motors are trying to move the telescope through it’s search pattern most of the time. The reduced temperatures affect the motors ability to produce torque; hence, the



(a) Quiet period from 21:30:20 for over 20 seconds.



(b) P10 heavy motor jitter from 21:35:00 over 20 seconds.



(c) P10 back to nominal operations from 21:37:15 over 20 seconds.

Figure 15: Pressure fluctuation data over various stages of P10's activity.

motor coils will be continuously charging and dis-charging (creating vibrations) but with limited torque and no shaft rotations. The cold temperatures decrease the magnetization level of the coils (leading to motor jitter). Furthermore, the cold temperature may cause internal lubrication to become more viscous, thus requiring more torque. The extended exposure to the cold may have also effected the other electronics (logic gates, MOSFETS, relays, etc.), the harmonic drive, and indeed any bearings and associated drive train. Lastly, the motors may need to operate with different duty cycles at different stages of the flight (motor temperature dependent).

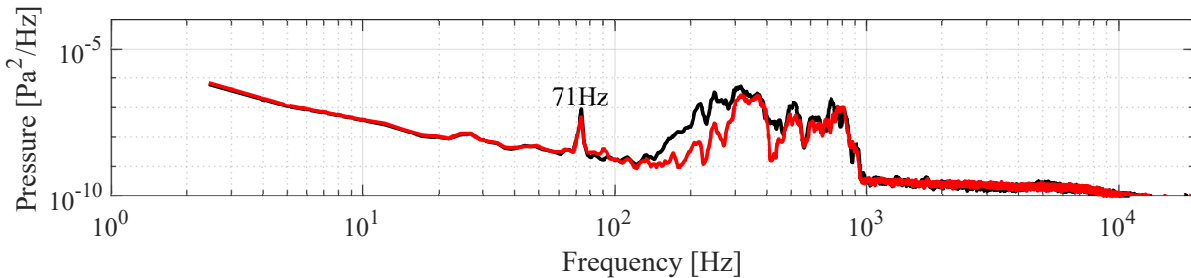


Figure 16: Data shown is 20 seconds from 16:58:00; 71Hz peak.

### 5.3.2 Acoustic Interference from P10

In order to attempt to separate acoustic interference from possible atmospheric pressure fluctuations we have to fully understand, to the best of our ability, noise from non-atmospheric sources. This is especially true for P10 as it is persistent and dominates all other pressure fluctuations. A little under half way through the CSBF float, at  $\approx 19:00:00$ , provides the quietest period of time in terms of atmospheric pressure fluctuations. At this time only pressure fluctuations caused by P10 acoustics are observed. Figure 17 presents particularly clean acoustic signals detected by both microphones from P10 over a 10 seconds starting at 19:00:00. It is emphasized that this interference pattern from P10 is observed in 99.4% of all pressure fluctuation data recorded by HAAT. Through private communications, P10 is understood to have identical drives for pitch and yaw, hence it is not clear if these will produce differing acoustic signatures. Pressure fluctuation data demonstrates sharp peaks occurring at approximately 1.6s intervals ( $\approx 0.625Hz$ ), inbetween which seven smaller/softer pulses with the same spectral content are observed. The frequency content is not observed to change, only the amplitude of the signal. Each of the pressure pulses observed are bounded by periods of quiet, and occur at frequency of  $\approx 5Hz$ . Unfortunately the frequencies produced by the neighboring payloads cannot be simply filtered out of the pressure fluctuation data. The reason for this is they coincide with pressure fluctuation data that is of interest regarding the free field stratosphere, and so they inherently corrupt the pressure fluctuation measurements. Furthermore, we cannot decipher more information out of HAAT's acoustic data with out access to other payloads, such as P10, in order to interrogate the acoustic frequencies of the motors and natural frequencies of the payload's structure. Had the hot-wire survived ground logistics, launch, and ascent, we would have been able to infer atmospheric disturbances in the pressure fluctuation data.

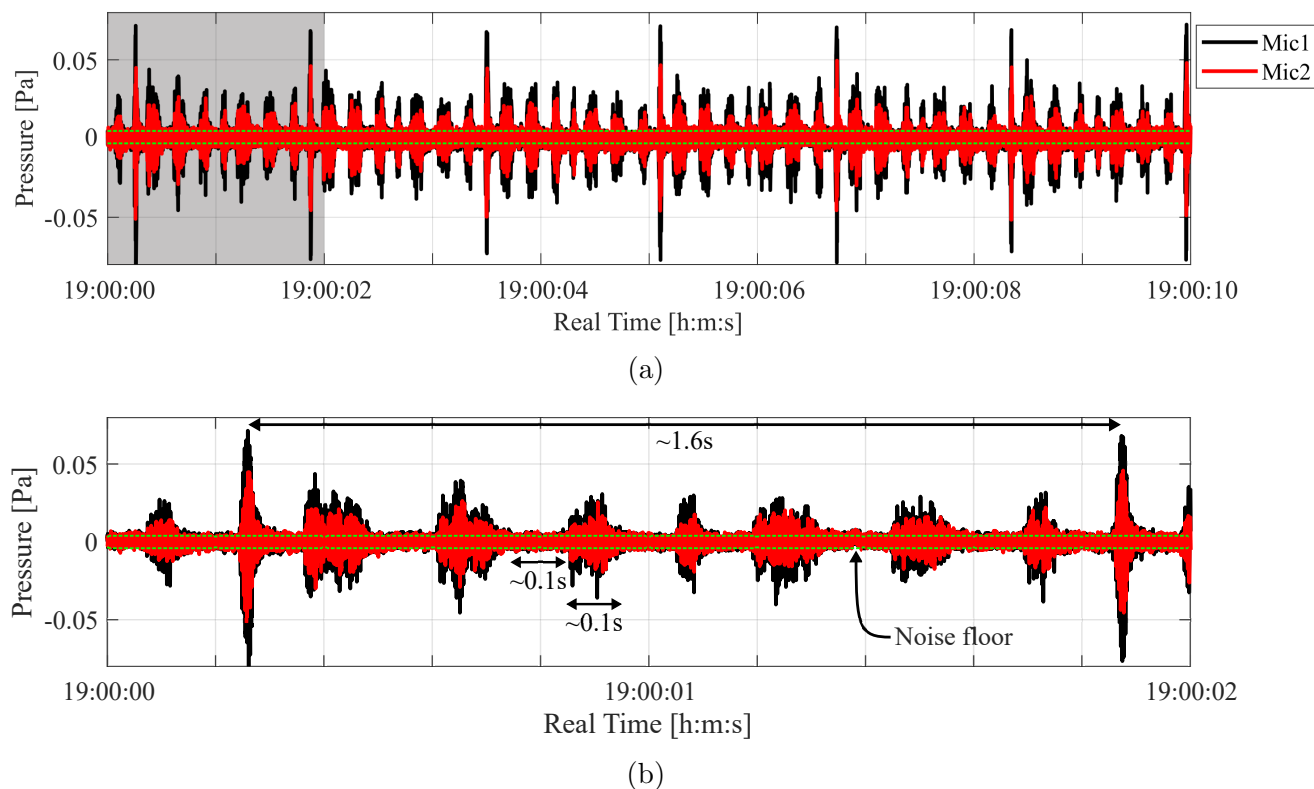


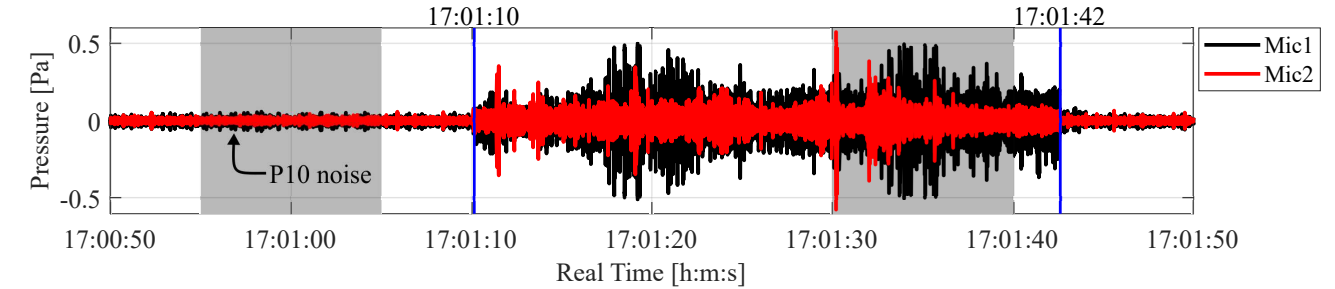
Figure 17: Pressure fluctuations detected by microphones 1 and 2 over a 10 second period at 19:00:00. This period time has particularly low background noise, producing a very clean acoustic signal coming from P10.

### 5.3.3 Pressure Fluctuations from Atmospheric Sources

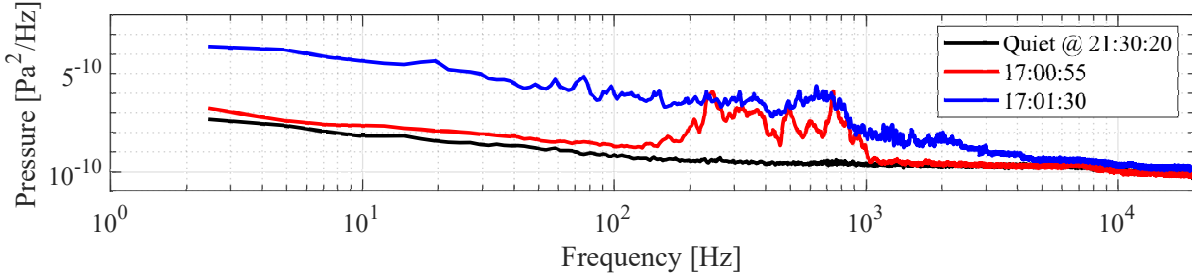
As discussed, the pressure fluctuation data is contaminated by nearby payloads. For this reason, it is not possible to investigate atmospheric pressure fluctuations that are of similar magnitude and frequency. However, during HAAT’s period of data acquisition, there are at least four occasions that have been identified in which the background atmospheric noise dominates the acoustic measurement. The most notable of which has been presented in figure 18a, between 17:01:10 and 17:01:42. It should be noted that though inspection of the CSBF feed these bursts in pressure fluctuation activity do coincide with gondola rotations (although likely driven by wind). It is also a possibility that broadband fluctuations are created by the dropping of ballast from underneath the main gondola, however the times over which ballast is dropped is not known.

The pressure fluctuations observed between 17:01:10 and 17:01:42 have peak pressure fluctuations of  $\approx 0.51Pa$  (an order of magnitude stronger than acoustic noise from P10). Figure 18b presents the three spectra: 1) from 21:30:20 which was the quietest point in the flight; 2) typical noise observed from P10 recorded at 17:00:55; and 3) a burst in pressure fluctuations overlaying P10’s fluctuations at 17:01:30.

As expected, the acoustic data taken over 17:01:30 (indicated by the blue curve) is contaminated by P10’s noise. This is evident by the humps in the spectra between 300Hz 1000Hz. Nevertheless, spectra content up to 5000Hz is observed, although the nature/cause of the pressure fluctuations is largely unknown.



(a) Pressure fluctuations recorded between 17:00:50 and 17:01:50



(b) Pressure fluctuation data from microphone 1 at three distinct times during the flight.

Figure 18: Temporal and spectral pressure fluctuation data detected by microphones 1 and 2. Spectral data illustrated three data sets indicating low noise, P10 noise, and P10 noise plus atmospheric pressure fluctuations.

## 6 Recovery

It is appreciated that the recovery of the CSBF gondola was particularly difficult due to premature flight termination, leading to the gondola landing on top of a butte North-West of Bluff, UT; however, critical pieces of equipment (specifically the hot- and cold- wire probe) were lost during recovery. Images and videos taken at the recovery site indicate that the wire sensors were still intact post impact, and personal communications have also confirmed that the sensors were installed in HAAT at least in the initial recovery

effort. Furthermore, inspection of HAAT’s probe supports indicate that the probes were taken out manually as locking mechanisms had been loosened but were still aligned with the vertical. Data logged during the flight indicates that the sensors were intact, but the wire damaged.

If HAAT operates with wire probes as a HASP payload with CSBF in the future it is highly recommended that personnel from UMD attend recovery operations to be responsible for the sensor recovery. If personnel from UMD are unable to attend, every effort should be made by the UMD team to identify specific personnel attending recovery operations to be responsible for the sensor recovery.

## 7 Conclusions

The University of Maryland UMD 2019 HASP team sought to combine the capability and fidelity of the High Altitude Atmospheric Turbulence (HAAT) payloads that previously flew in the 2017 and 2018 HASP campaigns. The continued development to HAAT has led to a balloon-borne payload capable of measuring turbulent fluctuations of velocity, temperature, and pressure (as well as mean temperature and pressure) in the stratosphere from the NASA Columbia Scientific Balloon Facility. Owing to the high spatial of  $2mm$ , turbulent velocity and temperature spectra can be studied down to the viscous sub-range, where the wire probes enable the investigation of disturbance length-scales relevant to hypersonic boundary-layer instabilities; i.e. wavelengths on the order of millimeters to centimeters. This would have enabled the statistical determination of the energy dissipation rate, thus facilitating a means to estimate the strength of turbulence without hot-/cold-wire calibrations; however, both the hot-and cold-wire probes were damaged before data acquisition was initiated. The high-sensitivity microphone enabled the interrogation pressure fluctuations down to  $\pm 0.004Pa$  for 5.19 hours during float. Examination of this data emphasized the sensitivity of our microphones to all ambient pressure fluctuations (and possibly mechanical vibration) as 99.4% of data is contaminated by non-atmospheric noise radiating from neighboring payloads.

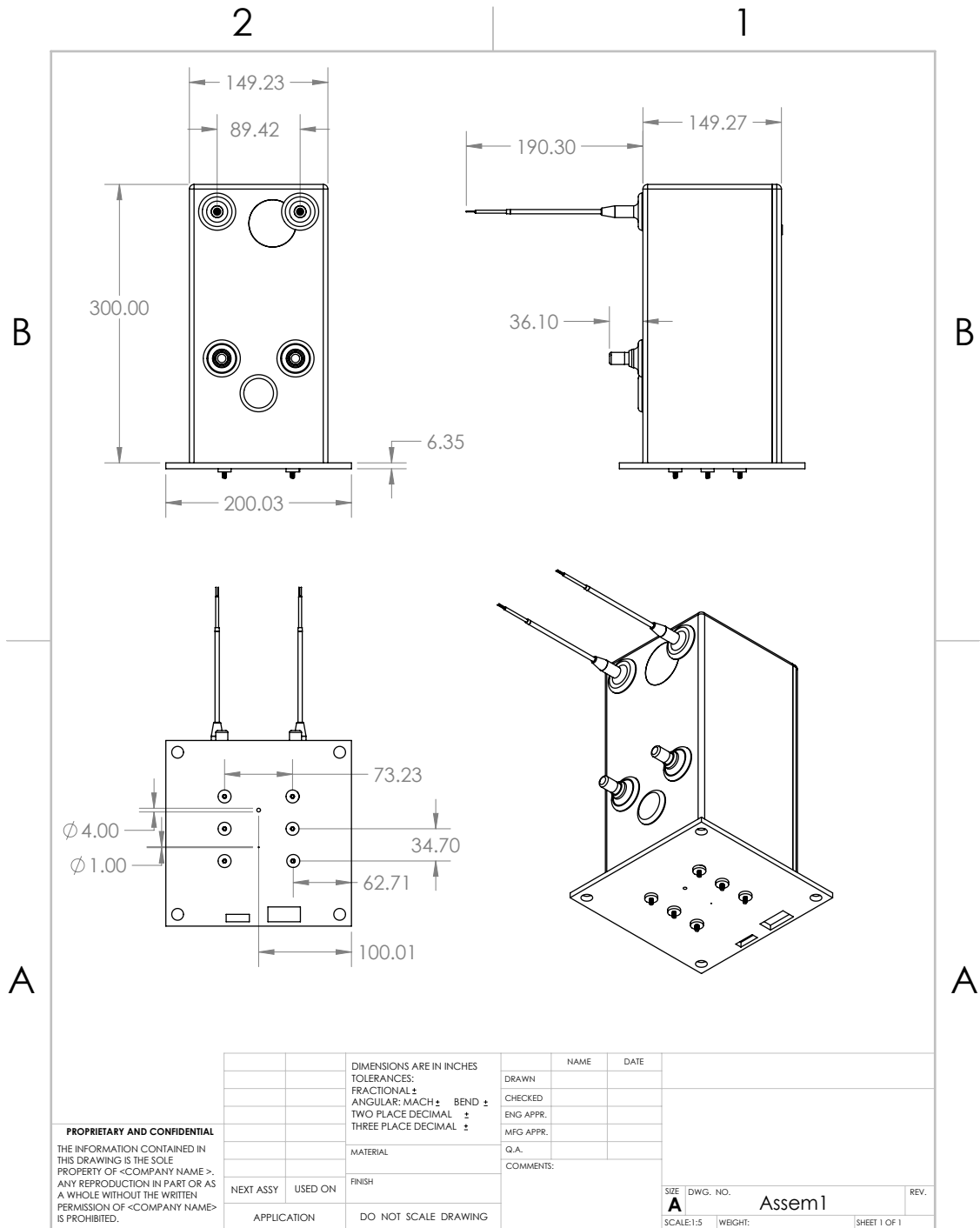
HAAT operated as intended for the full duration of the flight, although more information in the telemetry downlink during data acquisition would have been useful. Operators were completely reliant on current draw information (given by CSBF) and the output status of the data acquisition system to determine the operational functionality of the payload during the flight. This led to unnecessary power cycling of HAAT, stemming from operators trying to address an intermittent issue with the payload. This issue did not effect the payloads performance. The mechanical design, and integrated passive thermal management, also performed well with no issues to report. It is noted however, that had HAAT operated for a much longer period of time it may have overheated. Future designs will not incorporate as aggressive thermal management strategies.

HAAT was found to have unique problems to address for future operations with CSBF. The pressure fluctuation data (acoustic measurements) are strongly affected by the operations of neighboring HASP payloads, especially if they operate stepper motors. The temperature and velocity measurements will not be affected by other payloads, although steps should be made in the payload design/integration and launch logistics to improve the survivability of the wire probes. It is unrealistic for HAAT/UMD to impose requirements on other payload’s modes of operation. Hence, future iterations of HAAT will have to address how to directionally measure pressure fluctuation data, *i.e.* measure pressure fluctuation data in front of HAAT while directionally isolating measurements coming from nearby payloads. The immediate issue with this is that techniques employed (e.g. wave guides) will inherently make noise and may also modify the acoustics being measured.

Perhaps, a potential component of the solution to this problem would be to request a re-arrangement of payloads at integration in-order to position HAAT as far as possible from known sources of noise. Furthermore, time could be requested at integration to hold low pressure and temperature conditions for an extended period of time, in as quiet as possible ambient conditions. This may not be feasible as it does impose HAAT’s individual requirements on other payloads, and additionally, it is not known how quiet the thermal-vac tests conducted in Palestine, TX, can be. Assuming that the environmental chamber

can be effectively turned off once at appropriate temperature and pressure conditions, the background noise (e.g. personnel moving around, building climate control, vehicles outside, vibrations into/through the environmental chamber structure, etc.) may prove too high to provide meaningful measurements of neighboring payload noise. The practicality of these possible solution will have to be explored in the future. It may only be possible to assess other payloads one-by-one under sea-level conditions in order to determine separate acoustic signatures. Future UMD HASP teams, if flying high sensitivity microphones, should investigate possible avenues of understanding combined CSBF mechanical noise from nearby stepper motors, fans, and pumps to the best of their ability before the flight from Fort Sumner. Lastly, another solution may be to mount the microphones arrays in payloads situated in a ladder inbetween the main gondola and the parachute, such as that achieved by Bowman et al. [23, 24] in HASP 2014 and 2015.

# A Technical Drawings



SOLIDWORKS Educational Product. For Instructional Use Only.

Figure 19: Technical schematic of HAAT on HASP mounting plate. Dimensions in mm.

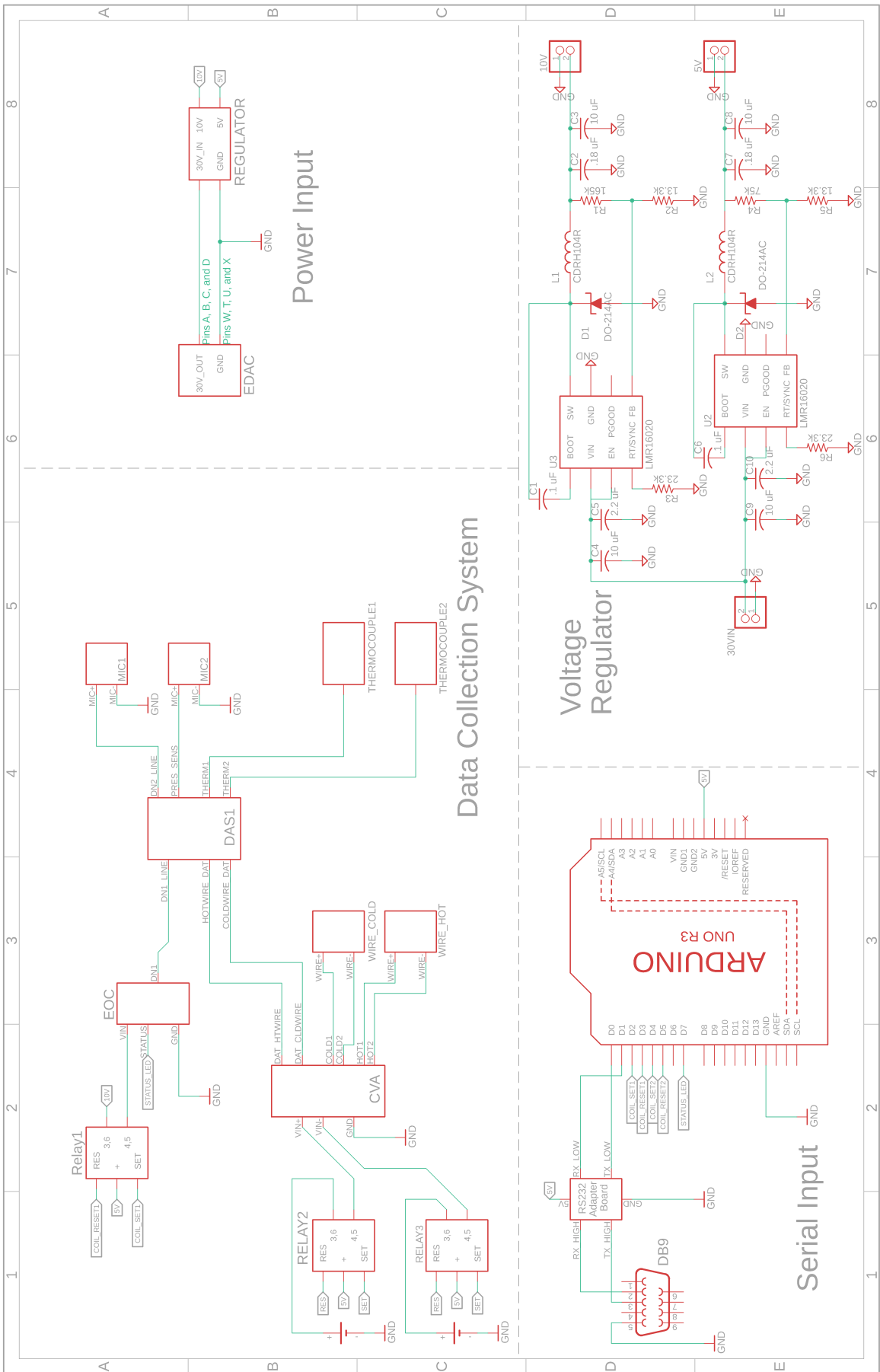


Figure 20: HAAT electronics schematic.

## B Flight Time-line

<b>Time</b>	<b>Event</b>
12:30:28	CSBF on / HAAT on
13:03:15	Launch
15:13:41 - 15:33:01	CSBF power cycle
15:40:37	Start of float
15:48:29	HAAT starts data acquisition
18:24:10	Current indicated to drop
18:41:06 - 18:41:37	HAAT power cycle
18:41:50	HAAT on
18:47:43	HAAT starts data acquisition
19:07:22	Current indicated to drop
19:17:58 - 19:18:11	HAAT power cycle
19:21:46	HAAT on
19:22:16	HAAT starts data acquisition
19:36:46	Current indicated to drop
19:43:43 - 19:44:02	HAAT power cycle
19:44:04	HAAT on
19:47:09	HAAT starts data acquisition
20:44:16	Oscillations in current draw start
21:11:03	Current indicated to drop
21:12:38 - 21:13:21	HAAT power cycle
21:13:32	HAAT on
21:19:23	HAAT starts data acquisition
21:50:14	HAAT runs out of free flash memory
23:17:56	Flight Termination
23:57:03	Impact

Table 3: Tabulated flight summary.

## C HAAT Pre- and Post-Flight



Figure 21: HAAT in the hanger at Fort Sumner just before launch.



Figure 22: HASP recovery, note the white ribbon tangles around the probe supports.

## D Full Team Personnel for HASP 2019

Table 4: Full team personnel for HASP 2019.

Name	Start Date	End Date	Role	Student Status	Race	Ethnicity	Gender	Dis-abled
Cameron Butler	11/15/16	Present	Graduate Science Lead	Graduate	White	Non-Hispanic	Male	No
Lorenzo Narducci	11/15/16	Present	Undergrad Student Lead	Undergrad	White	Non-Hispanic	Male	No
Jessica Queen	12/01/17	Present	Electronics and Systems Lead	Undergrad	White	Non-Hispanic	Female	No
Arnold Chonai	09/15/15	Present	Electronics	Undergrad	Asian	Non-Hispanic	Male	No
Quinn Kupec	11/15/16	Present	Mechanical Lead	Undergrad	White	Non-Hispanic	Male	No
Tiffany Ramcharan	09/15/15	Present	Mechanical Design and Thermal Management	Undergrad	Asian	Non-Hispanic	Female	No
Theo Kuiper	03/03/18	Present	Mechanical Design	Undergrad	White	Non-Hispanic	Male	No
Matthew Fowler	11/15/17	Present	Sensor Integration and Software	Undergrad	White	Non-Hispanic	Male	No
Zachary Burnett	11/15/16	Present	Sensor Integration and Software	Undergrad	White	Non-Hispanic	Male	No
Shaun Skinner	11/01/18	Present	Project Manager (Post-Doc)	N/A	White	Non-Hispanic	Male	No
Arun Mangalam	11/15/16	Present	Industry partner (Tao Systems Inc.)	N/A	Asian	Non-Hispanic	Male	No
Mary Bowden	2000	Present	Faculty Advisory	N/A	White	Non-Hispanic	Female	No
Stuart Laurence	2013	Present	Faculty Advisory	N/A	White	Non-Hispanic	Male	No

Table 5: Key personnel contact information for HASP 2019.

Dr. Shaun Skinner	Project Manager	skinner1@umd.edu
Cameron Butler	Graduate Science Lead	cameron.mech@gmail.com
Lorenzo Narducci	Student Lead	lzonarducci@gmail.com
Dr. Mary Bowden	Faculty Adviser	maryb@ssl.umd.edu
Dr. Stuart Laurence	Faculty Adviser	stuartl@umd.edu

## E Placement of Students from Past UMD HASP Teams

Many of the students who worked on HASP in past years are now research assistants in a graduate program or working in the aerospace field in a number of different locations and capacities:

- Lorenzo Narducci, NASA Goddard Space Flight Center
- Blaire Weinberg, Jet Propulsion Lab
- Michael Owca, Systems Engineering Group (SEG)
- Jessica Queen, Intern at NASA Goddard Space Flight Center
- Dru Ellsberry, first SpaceX now Blue Origins
- Connie Ciarleglio, first JPL now SpaceX
- Kristy Weber, University of Colorado Boulder Graduate Program
- David Thoerig, NASA Johnson Space Center
- Chris Carlsen, Blue Origins
- Camden Miller, Jet Propulsion Lab
- Jackson Phillips, Innovative Concepts Engineering
- Steve Lentine, contractor at Goddard Space Flight Center
- Bianca Foltan, Northrop Grumman Innovation Systems
- Tyler Boyle, Glenelg Country High School Science teacher
- Ji Min Chang, Textron Aviation
- Mohammed Nassif, Georgia Tech Graduate School
- Chukwuma Odigwe, FAA Unmanned Aircraft Systems
- Michael Walker, NASA Goddard Space Flight Center

Besides being a very valuable undergraduate experience that helps our graduating seniors find jobs in the aerospace field, the HASP Program has also provided participating students with ballooning experience that they then bring back to the much larger team of UMD students. This facilitates the building of future payloads and performing balloon launch operations for our local Balloon Payload Program. This program has been underway for 16 years, involving hundreds of undergraduates, and several graduate students, with over 90 flights of sounding balloons launched in the central East Coast Region. The University of Maryland ballooning program has benefited significantly from numerous interactions with the NASA Balloon Program Office and the Columbia Scientific Ballooning Facility (CSBF).

## References

- [1] E. Reshotko. Boundary-Layer Stability and Transition. *Annual Review of Fluid Mechanics*, 8:311–349, 1976.
- [2] H. Ozawa, S.J. Laurence, J.M. Schramm, A. Wagner, and K. Hannemann. Fast-Response Temperature-Sensitive-Paint Measurements on a Hypersonic Transition Cone. *Experiments in Fluids*, 56(1):1–13, 2015.
- [3] S.P. Schneider. Effects of High-Speed Tunnel Noise on Laminar-Turbulent Transition. *Journal of Spacecraft and Rockets*, 38:323–333, 2001.
- [4] L. Duan, M. Choudhari, A. Chou, F. Munoz, R. Radespiel, T. Schilden, W. Schroder, E.C. Marineau, K.M. Casper, R.S. Chaudhry, G. Candler, K. Gray, and S. Schneider. Characterization of Freestream Disturbances in Conventional Hypersonic Wind Tunnels. *Journal of Spacecraft and Rockets*, 56(2), 2019.
- [5] E.C. Marineau, G. Grossie, A. Wagner, M. Leinemann, R. Radespiel, H. Tanno, R.M. Wagnild, and K.M. Casper. Analysis of Second-Mode Amplitudes on Sharp Cones in Hypersonic Wind Tunnels. *Journal of Spacecraft and Rockets*, 56(2), 2019.
- [6] S.P. Schneider. Development of Hypersonic Quiet Tunnels. *Journal of Spacecraft and Rockets*, 45(4):641–664, 2008.
- [7] W.M. Crooks, F.M. Hoblit, and F.A. Mitchell. Project HICAT: High Altitude Clear Air Turbulence Measurements and Meteorological Correlations. *Tech. Rep. AFFDL-TR-68-127*, Air Force Flight Dynamics Lab, 1, 1968.
- [8] C.L. Johnson. Development of the Lockheed SR-71 Blackbird. *CIA Report 3675-81*, 1981.
- [9] P.W. Merlin. Design and Development of the Blackbird: Challenges and Lessons Learned. In *47th AIAA Aerospace Sciences Meeting Including The New Horizons Forum and Aerospace Exposition: AIAA paper 2009-1522*, number January, 2009.
- [10] Airbus and Perlan. Perlan Project Partners with Airbus Group to Fly a Glider to the Edge of Space: Press Release. *Perlan Project Inc.*, 2014.
- [11] Airbus and Perlan. Airbus Perlan Mission II Glider Soars to 76,000 feet to Break Own Altitude Record, Surpassing Even U-2 Reconnaissance Plane: Press Release. *Perlan Project Inc.*, 2018.
- [12] D. Cadet. Energy Dissipation within Intermittent Clear Air Turbulence Patches. *Journal of the Atmospheric Sciences*, 34:137–142, 1977.
- [13] J. Barat. Some Characteristics of Clear-Air Turbulence in the Middle Stratosphere. *Journal of the Atmospheric Sciences*, 39:2553–2564, 1982.
- [14] J. Barat, C. Cot, and C. Sidi. On the Measurement of Turbulence Dissipation Rate from Rising Balloons. *Journal of Atmospheric and Oceanic Technology*, 1:270–275, 1984.
- [15] A. Theuerkauf. *Stratospheric Turbulence Observations with the New Balloon-Borne Instrument LITOS*. PhD thesis, University of Rostock, 2012.

- [16] A. Schneider, J. Wagner, J. Söder, M. Gerding, and F.J. Lübken. Case study of wave breaking with high-resolution turbulence measurements with LITOS and WRF simulations. *Atmospheric Chemistry and Physics*, 17(12):7941–7954, 2017.
- [17] F.J. Lübken, W. Hillert, G. Lehmacher, and U. von Zahn. Neutral Air Turbulence During DYANA: First Results. *Advances in Space Research*, 12(10):135–139, 1992.
- [18] P.C. Stainback and K.A. Nagabushana. Review of Hot-Wire Anemometry Techniques and the Range of their Applicability for Various Flows. *Electronic Journal of Fluids Engineering, Transactions of the ASME*, 167:1–54, 1993.
- [19] J.D. Norris and N. Chokani. Rapid Scanning of Overheat Ratios Using a Constant Voltage Anemometer. *AIAA Journal*, 41(8):1619–1621, 2003.
- [20] G.R. Sarma. Transfer Function Analysis of the Constant Voltage Anemometer. *Review fo Scientific Instruments*, 69(6):2384–2391, 1998.
- [21] M.A. Kegerise and E.F. Spina. A Comparative Study of Constant-Voltage and Constant-Temperature Hot-Wire Anemometers: Part II - The Dynamic Response. *Experiments in Fluids*, 29:165–177, 2000.
- [22] NASA. HASP – Student Payload Interface Manual; Version 02.17.09. Technical report, 2018.
- [23] D.C. Bowman, P. Gouge, T. Larson, J.F. Anderson, and J.M. Lees. 2014 High Altitude Student Platform (HASP) Balloons over Volcanoes Scientific Balloons over Volcanoes Scientific Report. Technical report, 2014.
- [24] D.C. Bowman. *Infrasound From Ground to Space*. Ph.d., University of North Carolina, 2016.